Dalton Transactions

Accepted Manuscript

ROYAL SOCIETY OF CHEMISTRY

www.rsc.org/dalton

Graphical abstract

The contrarotational fluxionality of [3,3-$(PMe_2Ph)_2$-*closo*-3,1,2-$PtC_2B_9H_{11}$] and related species

Robert D. Kennedy and John D. Kennedy

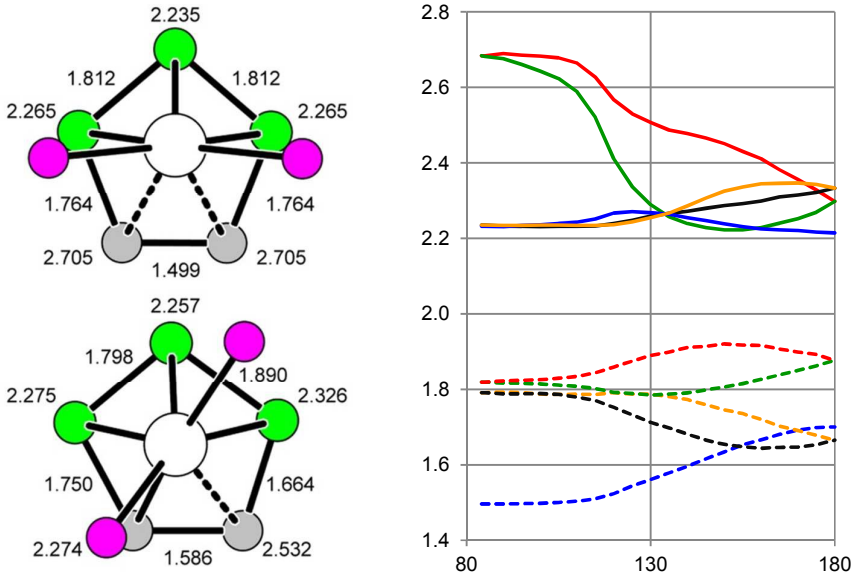

DFT calculations allied with experimental crystallographic and NMR results elucidate the energetics and the geometrical and ^{11}B nuclear shielding changes in the contrarotational fluxionality of [3,3-$(PMe_2Ph)_2$-*closo*-3,1,2-$PtC_2B_9H_{11}$] and confirm the incidence and identities of two stable rotational conformers.

The contrarotational fluxionality of [3,3-$(PMe_2Ph)_2$-*closo*-3,1,2-$PtC_2B_9H_{11}$] and related species

Robert D. Kennedy[a,b] and John D. Kennedy[b,c,*]

[a] Department of Chemistry and Biochemistry, University of California, Los Angeles, California 90095-1569, USA; Department of Chemistry, Northwestern University, Evanston, Illinois, 60208, USA.

[b] School of Chemistry, University of Leeds, Leeds, UK LS2 9JT.

[c] Institute of Inorganic Chemistry, Academy of Sciences of the Czech Republic, 25068 Řež u Prahy, The Czech Republic

* corresponding author; e-mail: j.d.kennedy@leeds.ac.uk

It is a privilege to be able to contribute to this Edition dedicated to the memory of Ken Wade, in celebration of his sustained and formidable contributions to chemical science, and in personal memory in particular of many friendly and stimulating discussions over the years, both relevant and irrelevant to chemical science.

Abstract

DFT calculations allied with experimental crystallographic and NMR results elucidate the energetics and the geometrical and ^{11}B nuclear shielding changes in the contrarotational fluxionality of [3,3-$(PMe_2Ph)_2$-*closo*-3,1,2-$PtC_2B_9H_{11}$] and confirm the identities of two stable rotational conformers. There is a relatively unhindered contrarotation of the $\{Pt(PR_3)_2\}$ and *nido*-shaped carbons-together $\{C_2B_9H_{11}\}$ entities about an axis that contains the platinum atom, with a transition from *trihapto* to *tetrahapto* to *pentahapto* metal-to-cluster interaction as the rotation progresses from 0º to 90 º, and a reversal as it progresses in turn through to 180º, and thence through a similar cycle through to 360º for a complete rotation. The overall energy minimum is the *trihapto* conformation, but there is also an island of stability for the *tetrahapto* conformation at slightly higher energy, corresponding to experimental observation of these two configurations. The highest-energy *pentahapto* mode constitutes a transition state, and its energy defines the activation energy for the complete contrarotation, which is matched by activation energies derived from NMR spectroscopy. The shallow minima and small energy differences suggest that ready cluster flexibility will be expected about the minima, again in accord with subtle rotamer angle differences seen in experimental results. Nuclear magnetic shielding criteria suggest significant changes in intracluster bonding as the rotation progresses. The *trihapto* bonding geometry and the corresponding electronic structure are favoured over quite a substantial arc (some 40º) of the rotation, before rapid changes ensue, and then, after progression through the *tetrahapto* conformation, the electronics and the bonding geometry then again remain similar within the *pentahapto* mode for a further 40º or so of the rotational arc about this transition state.

Introduction

Half a century ago Hawthorne and co-workers discovered that the formal [*nido*-7,8-$C_2B_9H_{11}]^{2-}$ dianion (schematic cluster structure **I**, *nido* eleven-vertex numbering scheme as in **IA**), often subsequently called the 'dicarbollide' ligand, could bind to transition-element centres to generate closed icosahedral clusters of deltahedral character (schematic cluster structure **II**, *closo* twelve-vertex numbering scheme as in **IIA**).[1]

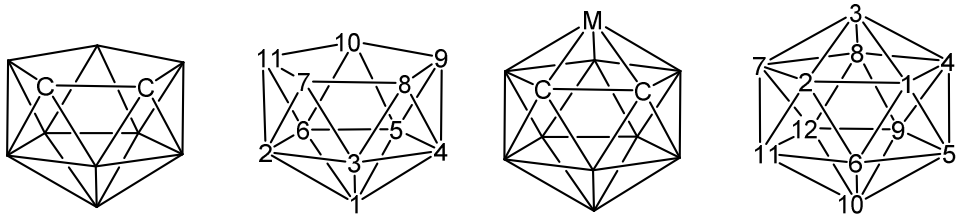

I **IA** **II** **IIA**

The resulting 'metal dicarbollides', formally *closo*-3,1,2-metalladicarbaboranes, now constitute one of the most examined areas of boron-containing cage and cluster chemistry, surpassed only by that based on [*closo*-$C_2B_{10}H_{12}$] species.[2] As the area developed it became recognized that not all metal centres formed closed triangulated icosahedra when coordinated to the *nido*-shaped {7,8-$C_2B_9H_{11}$} unit,[3] and Colquhoun and Wallbridge subsequently described an elegant sequence of compounds in which the binding of the dicarbaborane unit to the metal centres progressed from *pentahapto* (as in schematic cluster structure **II**), through degrees of increasingly less involvement (schematic cluster structures **III** to **VI**), to a looser general association (schematic cluster structure **VII**), as the nature of the metal centre progressed from the centre of the transition series to the late transition elements and thence to the post-transition elements mercury (**VI**) and thallium (**VII**).[4]

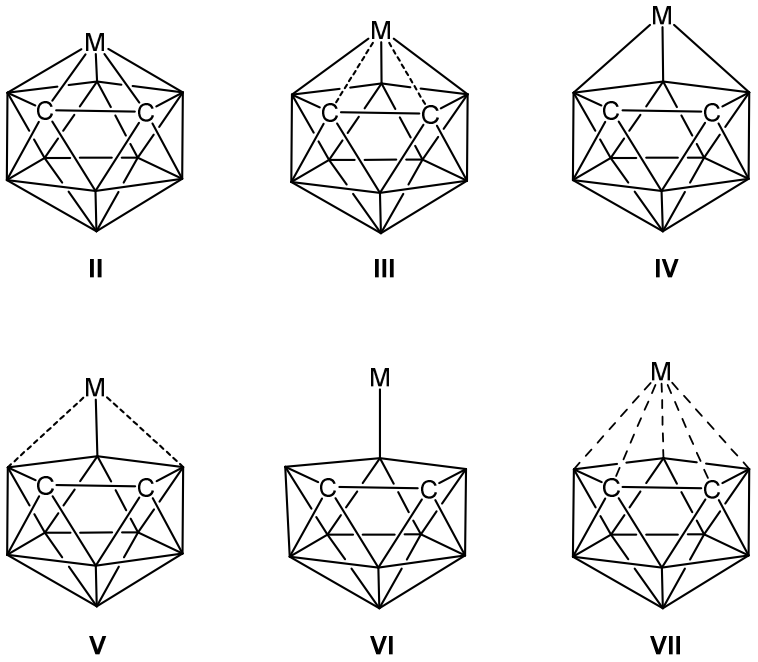

II **III** **IV**

V **VI** **VII**

They made the point that 'any attempt to predict metallacarborane structures on the basis of electron-counting rules must take into account the electron configuration of the metal in its formal oxidation state, at least for the heavier transition and post-transition elements' - interestingly, nearly some forty years on, this and related points are still not generally appreciated [see, for example, ref 5 *versus* refs 6 and 7]. In the general context of 'stretching' of the {$MC_2B_9H_{11}$} framework, it should be noted that an interesting alternative cluster opening is the stretching of the intercarbon distance (schematic cluster structures **II**→**VIII**→**IX**), rather than the metal-to-carbon distances,[8] and this has been addressed recently using {$ArRuC_2B_9H_{11}$}-based compounds as the examples.[9] However, this last phenomenon is orthogonal to the work that we describe in this present paper.

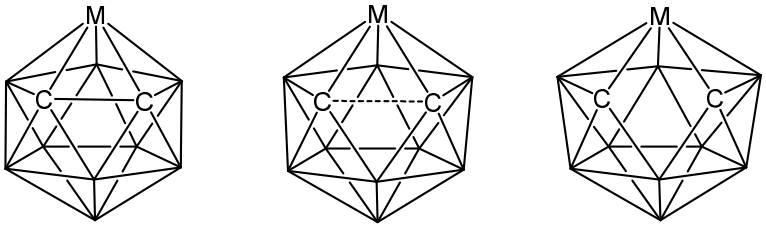

II **VIII** **IX**

In terms of this present contribution, within the sequence of progressive opening **II – VII** the configuration **III** has attracted significant attention, with particular reference to its so-called 'slippage' away from the completely triangulated configuration **II**.[10] For $[L_2PtC_2B_9H_{11}]$ and $[L_2PdC_2B_9H_{11}]$ species,[11,12] the slipped configurations exhibited in the solid state, as determined by X-ray diffraction analyses, were rationalised some time ago in terms of a frontier orbital approach.[12] Subsequently it became apparent that such species are very fluxional in solution with regard to an effective contrarotation of the $\{PtL_2\}$ and $\{PtC_2B_{10}H_{11}\}$ moieties about an axis that approximately contains the metal atom and its antipodal cluster atom B(10) (simplistic illustrative diagram **XA**).[13] The species $[(PMe_2Ph)_2PtC_2B_9H_{11}]$ is the best examined for contrarotational fluxionality: the activation energy $\Delta G^{\ddagger}$ was found to be $\leq$ *ca.* 30 kJ mol^{-1}. It is convenient to regard the contrarotation in terms relative to a quasi rotating frame of the dicarbaborane unit (schematic **XB**); in this model the $\{ML_2\}$ metal-centre unit rotates above the five-membered 'open face' of a static non-rotating $\{C_2B_9H_{11}\}$ entity.

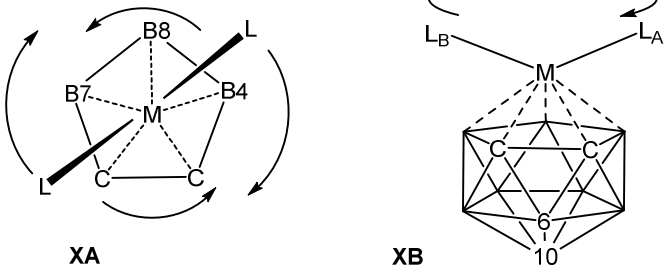

XA **XB**

Interest was added when it became apparent that different compounds exhibited significantly different contrarotamer rotation angles in the solid state,[14] and, further, that the species $[(PMe_2Ph)_2PtC_2B_9H_{11}]$ exhibits two very different contrarotamers in the *same* solid-state crystal structure (Figure 1 below).[15] Additionally, it was also apparent that the As_2 analogue $[(PEt_3)_2PtAs_2B_9H_9]$ also has a very low-energy rotational fluxionality in solution and, further, in the solid-state, effectively exhibits five different rotamers.[15,16] It was proposed that a mechanism for the rotation of the $\{Pt(PR_3)_2\}$ units above the faces of the *nido*-shaped eleven-vertex heteroborane units involved changes in effective metal-to-heteroborane hapticity among η^3 *trihapto*, η^4 *tetrahapto* and η^5 *pentahapto*.[15] The earlier frontier molecular-orbital approach on the dicarbametallaborane species did not deal with the relative energetics and dealt principally with the parallel configuration,[12] and in view of the observed rotational fluxionalities and the subsequently discovered tendency to exhibit more than one observable rotamer, we thought it informative to examine the energetics of the rotational phenomenon by DFT calculation, and to similarly examine for the nature of any concomitant change in carbaborane-to-metal hapticity as the rotation progresses. At this point, in the more general context of computational studies of contrarotational

processes involving the $\{C_2B_9H_{11}\}$ ligand unit, the seminal pioneering work of Bühl and coworkers on (non-slipped) transition-element bis(dicarbollide) species should be well noted.[17]

Results and Discussion

The two uppermost diagrams of Figure 1 show the experimentally observed conformation for $[(PEt_3)_2Pt\text{-}C_2B_9H_{11}]$,[12] and the corresponding conformation for one of the rotational isomers observed in the solid-state structure of $[(PMe_2Ph)_2PtC_2B_9H_{11}]$.[15] These approximate to a 'parallel' configuration, so-called because in the ideal case it was supposed that the P–P vector might parallel the intercarbon vector; this conformation has generally been regarded as the more stable, and formed the basis for the original frontier orbital considerations that were invoked to rationalise this observed configuration.[12] The lower diagram shows the second of the two conformations subsequently seen in the solid state structure of $[(PMe_2Ph)_2PtC_2B_9H_{11}]$, the 'diagonal' conformation.

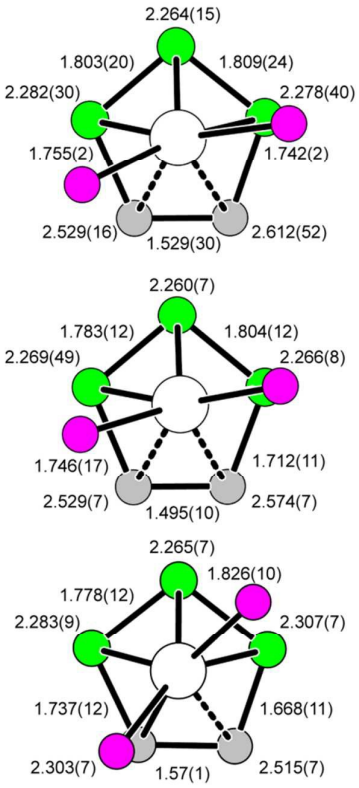

Figure 1. Projections of the crystallographically determined molecular structures of (top left) $[(PEt_3)_2PtC_2B_9H_{11}]$ [data from ref. 12], (top right) one of the two independent molecules in the crystal structure of $[(PMe_2Ph)_2PtC_2B_9H_{11}]$, which show the 'parallel' conformation, and (bottom) the second independent $[(PMe_2Ph)_2PtC_2B_9H_{11}]$ molecule [data from ref 15], which shows the 'diagonal' conformation. Hydrogen atoms, P-organyl groups, and the lower six {BH(*exo*)} units are omitted for clarity. Distances from platinum to carbon or boron are given next to the relevant carbon or boron atom and distances between carbon and / or boron atoms are given adjacent to the relevant connector.

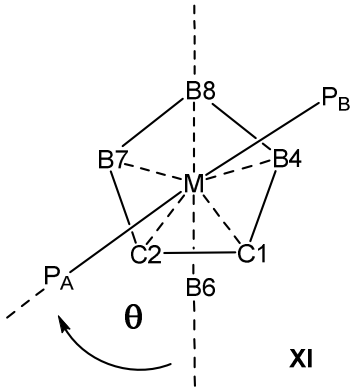

XI

Initial calculations were carried out for the model compound $[(PH_3)_2PtC_2B_9H_{11}]$. The PBE hybrid functional in Gaussian03 was used,[18] with the 6-31G(d) basis sets for C, H, B and P, and the Stuttgart-Dresden ECP plus double-zeta basis set for Pt. The initial starting $\{P_2PtC_2B_9H_{11}\}$ geometry was taken from the single-crystal result for $[(PMe_2Ph)_2PtC_2B_9H_{11}]$, and calculations were carried out for a succession of constrained angles of rotation, taking increments of 5º, the rotational angle being defined as the dihedral angle between the Pt–P_A and B(6)–B(10) vectors. This angle *approximately* relates to the angle **θ** in schematic structure **XI**. The energetic results are in Figure 2, which also shows the variation of the complementary dihedral angle between the Pt–P_B and B(6)–B(10) vectors. Two aspects arise out of the use of the incremental method of calculation and the use of the dihedral angle constraint for this. First, the curve is not symmetrical about 90º, the minimum being in fact at *ca.* 84º. This is because there is cluster flexing and in addition the dihedral angle does not map directly onto the simplistic projection angle **θ** of schematic structure **XI**, in that, for example, B(10) is not in the plane defined by P-Pt-P. Second, the plot of the complementary dihedral angle should in principle be linear, but is clearly not so; this arises because of Pt–PH_3 rotamer considerations, which result in structural 'flips' as the PH_3 groups pass through positions that eclipse the BH and CH positions on the pentagonal frontier face of the $\{C_2B_9H_{11}\}$ unit; these steric considerations also seem associated with a tendency to have stable 'diagonal' conformations (e.g. bottom diagram in Figure 1) at approximately 50º and 130º as mentioned below.

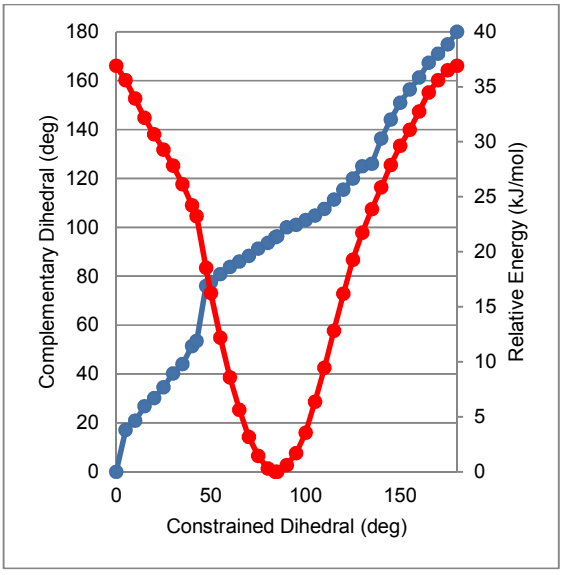

Figure 2. Plots of (red trace) calculated molecular energies a *versus* the constrained contrarotation angle based on B(6)-B(10)-Pt-P_A for the model compound [$(PH_3)PtC_2B_9H_{11}$] and (blue trace) the complementary rotation angle based on B(6)-B(10)-Pt-P_B in the resulting calculated structures.

The plot clearly demonstrates a global minimum energy; this corresponds to a rotational angle of 84º. This approximates to the 'parallel' conformations exhibited in the solid state by [$(PEt_3)_2PtC_2B_9H_{11}$] (73º) and also by one of the two independent molecules in the crystal structure of [$(PMe_2Ph)_2PtC_2B_9H_{11}$] (78º) (Figure 1, uppermost diagrams). It also clearly shows a maximum value at 0º / 180º, which would correspond to a contrarotational transition state in which one of the PH_3 ligands eclipses the BH(8) position and the other is over the middle of the C(1)–C(2) vector - a 'perpendicular' conformation. This global maximum is at 37 kJ mol^{-1} above the global minimum, and would correspond to an activation energy $\Delta G^{\ddagger}$ of this value for a rotational process. This is somewhat greater than the maximum value of *ca.* 30 kJ mol^{-1} inferred from solution studies on the [$(PMe_2Ph)_2PtC_2B_9H_{11}$] analogue;[13,15] however, this calculated value is for an isolated 'gas-phase' species, as opposed to the experimental result from solution state in a polar solvent, and there will also be differential electronic and steric effects arising from PMe_2Ph *versus* PH_3.

For this model [$(PH_3)_2PtC_2B_9H_{11}$] system there are no intermediate-energy minima at rotational angles around *ca.* 50º and 130 º, contrary to expectations for a 'diagonal' conformer equivalent to that observed for the second conformer in the crystal structure of [$(PMe_2Ph)_2PtC_2B_9H_{11}$] (Figure 1, bottom diagram). There are, however, weak inflexion points on the plot at these approximate angles, at about 25 kJ mol^{-1} above the global minimum. These presumably result from an unfulfilled tendency to favour such a configuration, a tendency possibly helped by an imminent mini-barrier as the PH_3 groups approach the steric step of eclipsing the carbaborane {CH} positons. This tendency is obviously better fulfilled for [$(PMe_2Ph)_2PtC_2B_9H_{11}$], as evidenced by the diagonal conformer actually present in the solid state for this species. Again, electronic differences between PH_3 and PMe_2Ph will be of importance, as well as crystal-packing effects within the solid-state crystal of [$(PMe_2Ph)_2PtC_2B_9H_{11}$]; here it is noted that intermolecular interactions and differential electronic ligand effects have been shown to be of high significance in dictating rotamer angles in closely related solid-state palladium systems.[14]

Compared to PH_3, steric effects are greater and electronic effects different for increasingly bulkier PMe_3 and PMe_2Ph. [$(PMe_3)_2PtC_2B_9H_{11}$] has not yet been reported, but we used it as the most convenient progressive model for triorganylphosphine ligands. For reasons of computational and time economy resulting from limitations of available hardware, extensive optimisations were not feasible for [$(PMe_3)_2PtC_2B_9H_{11}$], and, also, a full 180º sequence, in which Pt–PMe_3 rotamers and inter-ligand meshing are involved, was not conducted. For [$(PMe_3)_2PtC_2B_9H_{11}$], rather, we focused on the 'perpendicular' transition state, the global-minimum 'parallel' conformation, and the points around the 'diagonal' configuration at a rotational angle of *ca*. 45º. The highest-energy perpendicular conformer, which would constitute the transition state for any contrarotation, was found at a rotation angle of 2º, and the global minimum occurred at 84º. This transition-state conformation was 33 kJ mol^{-1} above the energetic minimum, some 4 kJ mol^{-1} less than the 37 kJ mol^{-1} calculated for the PH_3 species. Extrapolation to more bulky PMe_2Ph would thence suggest a value less than 30 kJ mol^{-1}, which would be consistent with the solution-state experimental observations.

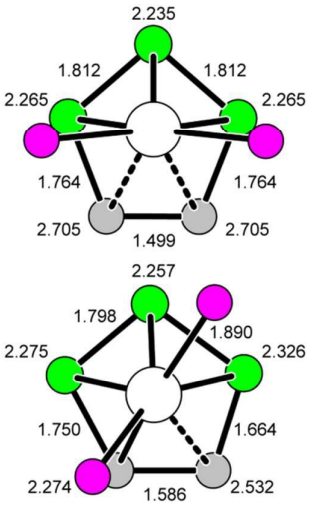

Figure 3. Projections of the molecular structures associated with the calculated energy minima for $[(PMe_3)_2PtC_2B_9H_{11}]$: (left) the lower energy 'parallel' minimum, and (right) the second 'diagonal' minimum at *ca.* 18 kJ mol^{-1} to higher energy. Hydrogen atoms, P-organyl groups, and the lower six {BH(*exo*)} units are omitted for clarity. It can be seen that the two rotamers closely resemble those found experimentally in the crystal structure of $[(PMe_2Ph_2)PtC_2B_9H_{11}]$ (Figure 1 above). Distances from platinum to carbon or boron are given next to the relevant carbon or boron atom and distances between carbon and / or boron atoms are given adjacent to the relevant connector.

For $[(PMe_3)_2PtC_2B_9H_{11}]$ the calculations also revealed a very shallow 'diagonal' minimum at 42º, with an energy 18 kJ mol^{-1} above the lowest-energy 84º conformer. Projections of the calculated parallel and diagonal minimum-energy structures are in Figure 3, and it can be seen that these closely resemble the corresponding experimentally found parallel and diagonal minima in $[(PMe_2Ph)_2PtC_2B_9H_{11}]$ [Figure 1 (lower)].

Calculations that we have been able to conduct for this latter more complex PMe_2Ph species itself, now with phenyl as well as methyl group rotamers involved, have been necessarily more limited because of computational time constraints. Again we concentrated on the areas around the parallel, diagonal and perpendicular conformations. The molecular structures of the resulting three configurations are illustrated in Figure 4. The parallel configuration calculated out as the fully unconstrained global minimum, and a transition state corresponding to the rotational pathway was located at 0°. This was at 30.6 kJ mol^{-1} above the global minimum, *i.e.* less than that calculated for the PMe_3 case, and in accord with the upper limit of *ca.* 30 kJ mol^{-1} for the rotational barrier found experimentally for the PMe_2Ph compound. For the diagonal conformation, we located a local minimum at 42º/129º , confirmed by frequency calculations; this is at +8.8 kJ mol^{-1} above the global minimum 'parallel' conformation. In view of the small energy differences and shallow potential wells, it is probable that solid-state packing will have a significant influence on dictating the precise angles to be observed in crystal structures.

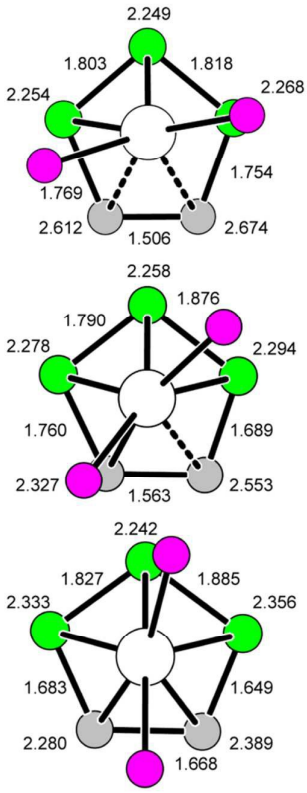

Figure 4. Representations of the calculated 'gas phase' molecular structures for $[(PMe_2Ph)_2PtC_2B_9H_{11}]$. Top, the global minimum 'parallel' conformation; centre, the 42º/129º 'diagonal' conformation at a relative energy of +8.8 kJ mol^{-1} ; bottom, the 'perpendicular' transition state at +30.6 kJ mol^{-1}.

Overall, the surmise about this rotational behaviour derived from experiment, for example in reference 15, is now more quantitatively supported, *viz.* there is a relatively low-energy rotational process progressing smoothly through the parallel, diagonal, and perpendicular conformations. The lowest-energy configuration is the 'parallel' one, and the highest-energy 'perpendicular' configuration dictates the rotational energy barrier. There is also a region of stability around the 'diagonal' configuration of intermediate energy, a few kJ mol^{-1} above the parallel configuration, and packing forces dictate that this is also sometimes observed in the solid state.

The surmise also proposed a switching among various carbaborane-to-metal hapticities as the rotation progressed .[15] Our results also provide insight into this. Available calculated and experimental interatomic distances and angles for the PH_3, PMe_3, PEt_3 and PMe_2Ph systems are given in the supplementary data (Tables S1-S3), and salient calculated values for $[(PMe_3)_2PtC_2B_9H_{11}]$ as representative are in Table 1. Inspection shows that the 84º global minimum is clearly η^3 *trihapto*, essentially consistent with the 'classically' slipped and experimentally well-substantiated configuration represented in **III** above, with the Pt–C distances at 2.705 Å much longer than the Pt–B distances of 2.235 and 2.265 Å . Upon swinging round to the 'diagonal' 42º conformer at the higher minimum, the hapticity now approximates closely to η^4 *tetrahapto*, with one longer Pt–C distance at 2.532 Å, and the other much shorter at 2.274 Å and within the range of the three Pt–B distances of 2.257, 2.275 and 2.326 Å. For the highest-energy near-symmetrical perpendicular configuration, for which frequency calculations confirmed its nature as the rotational transition state, the two Pt–C distances of 2.328 Å and 2.339 Å are very close to those of Pt–B(4) and Pt–B(7) at 2.349 Å and 2.350 Å , and Pt–B(8) is a little

shorter at 2.241 Å: this latter Pt–C and Pt–B grouping within a close range of *ca*. 0.2 Å can clearly be regarded as η^5 *pentahapto.*

As expected there is also general cluster flexing as the rotation progresses, with, for example, the intercarbon distances at 1.499, 1.586 and 1.674 Å, and the P–Pt–P angles at 104.5º, 97.8º and 100.25 º, respectively for the parallel energy minimum, the diagonal energy minimum and the perpendicular high-energy transition state. With regard to such cluster distortions associated with the slippage, the convex 'fold angle' of the frontier {C(1)C(2)B(7)B(8)B(4)} face receives considerable attention in earlier structural descriptions.[12,19] Thus, for the parallel conformation, the C(1) and C(2) atoms are considerably below the mean {C(1)C(2)B(7)B(8)B(4)} plane: the fold angle found by experiment for the originally described $Pt(PEt_3)_2$ species is +8.96 ± 0.02º. That for the similar parallel configuration in the crystal of the $Pt(PMe_2Ph)_2$ species is similar at +10.0 ± 2.0º. These foldings are matched by the values for the calculated minima for the PH_3, PMe_3 and PMe_2Ph species at +14.003º, +12.765º and +11.860º respectively. The PH_3 and PMe_3 values are possibly larger because they represent true 'parallel' structures, whereas the PMe_2Ph minimum is skewed way from that ideal. When the rotation progresses towards the diagonal the simple fold concept cannot be applied because of the marked asymmetry inherent in the twist. Thus, at the 'diagonal' minima, both experimentally and by calculation, carbon atoms C(1) and C(2) position themselves above and below the mean plane in the ranges +0.042 to +0.050 and –0.064 to –0.069 Å respectively, boron atoms B(4) and B(8) similarly relate to the mean plane in ranges +0.054 to +0.063 and –0.026 to –0.039 Å respectively, whereas B(7) is approximately coincident with the mean plane. In these diagonal structures the disposition of the carbon and boron atoms in the {C(1)C(2)B(7)B(8)B(4)} frontier face resembles the 'twist' conformation of cyclopentane. The full quarter-rotation to the symmetrical perpendicular transition state results in an essentially planar {C(1)C(2)B(7)B(8)B(4)} frontier face, with a slight concave fold angle of < –2º for all three calculated structures. Overall, corresponding matchings between experimental and calculated geometries also occur for the folding of the 'lower girdle' {B(5)B(6)B(11)B(12)B(9)} unit.[19]

Table 1. Selected interatomic distances (in Å) and angles (in º), as calculated for the lowest-energy 'parallel', the intermediate-energy 'diagonal', and the highest-energy 'perpendicular' conformations of the triorganylphosphine model compound $[(PMe_3)_2PtC_2B_9H_{11}]$.

Dimension	Parallel 84º / 84 º	Diagonal 42 º / 141 º	**Perpendicular** **2 º / 179 º**
Dihedral angle 1	84.469	42.006	2.37
Dihedral angle 2	84.393	141.266	179.49
Pt(3)-C(1)	2.705	2.274	2.328
Pt(3)-C(2)	2.705	2.532	2.339
Pt(3)-B(4)	2.265	2.275	2.349
Pt(3)-B(7)	2.265	2.326	2.350
Pt(3)-B(8)	2.235	2.257	2.241
C(1)-C(2)	1.499	1.586	1.674
C(2)-B(7)	1.764	1.664	1.659
B(7)-B(8)	1.812	1.890	1.860
B(8)-B(4)	1.812	1.798	1.854
B(4)-C(1)	1.764	1.750	1.662
Pt(3)-P_A	2.294	2.310	2.325
Pt(3)-P_B	2.294	2.261	2.236
Angle P-Pt-P	104.493	97.799	100.25

It is of interest to examine for the angular domains in which these hapticities may persist and at which points they may change during the course of the rotation. A plot of relevant interatomic distances versus rotational angle for the model compound $[(PH_3)_2PtC_2B_9H_{11}]$ is in Figure 4; this deals with the first quarter-rotation, this will be mirrored for the second quarter-rotation, and the resulting half-rotation behaviour will be duplicated for the full rotation (see Supplementary Data, Figure S5). Computational economy precluded the much more time-consuming calculations that would be needed for full quarter-rotations of the triorganylphosphine congeners $[(PMe_3)_2PtC_2B_9H_{11}]$ and $[(PMe_2Ph)_2PtC_2B_9H_{11}]$. Immediately apparent from the Pt–C and Pt–B distance behaviour in Figure 4 and Supplementary Figure S5 is a long *trihapto* domain centred around the central 84º minimum-energy point, *i.e.* there is little geometrical bonding change in this system within the rotational arc of ca. 50º between about 65º and 115º. Either side there is a steep change towards a specific and precise coming together of the three Pt–B and one of the Pt–C distances for the *tetrahapto* point at about 45º and 135º; thence there is a more gradual transition as the second Pt–C distance shortens to match its sibling, with the resulting *pentahapto* mode thence also quite well defined in that the Pt–C and Pt–B distances are within *ca.* 0.2 Å of each other over a rotational arc of about 40º. Comparison with the energy profile of Figure 2 above correlates the central *trihapto* bonding plateau with an energy change of about 10–15 kJ mol^{-1} through zero back up to 10–15 kJ mol^{-1} across the 50º rotational arc, and then the more rapid change into quite substantial geometrical changes through *tetrahapto* to *pentahapto* as the energy increases further.

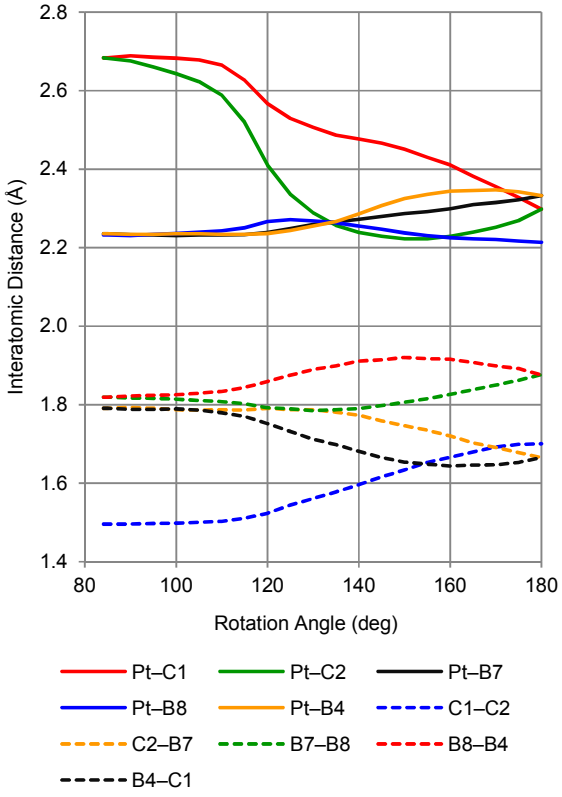

Figure 5. Plot of calculated interatomic distances *versus* rotational angle for the model species $[(PH_3)_2PtC_2B_9H_{11}]$. The long central plateau which corresponds to the *trihapto* parallel conformation is clear (< *ca.* 110º in this plot), and, interestingly, the *tetrahapto* points for the diagonal conformation are very well delineated in that the four relevant Pt–C and Pt–B distances are near-identical at the *ca.* 135º crossover angle. The close grouping of all five Pt–C and Pt–B distances around the

pentahapto perpendicular conformation is also very apparent. The diagram represents a quarter-rotation; the behaviour will be mirrored to represent a half-rotation, and the whole repeated to complete 360º rotation (Supplementary Data Figure S5).

It is also of interest to surmise whether the different conformations are associated with significantly different intracluster bonding.* Nuclear magnetic shieldings are intimately dependent upon molecular orbital structure,

---

* Footnote: a reviewer has suggested that 'the low rotational barrier is related to the relatively small separation in HOMOs derived from the e_1 degenerate set of the parent $\{B_{11}H_{11}\}$ anion.'

---

and thence significant changes in cluster electronics will be manifest in significant changes in cluster nuclear magnetic shielding properties. Conversely, and irrespective of the at present formidable task of determining which particular molecular-orbital changes may be dominant in dictating the observed changes in nuclear shieldings, significant changes in cluster nuclear magnetic shielding properties will give indication of significant changes in bonding. This approach has been applied successfully to a number of platinaboranes and platinacarboranes, for example systems based on formally *closo*-structured eleven-vertex [1,1-$(PR_3)_2$-1,2,3-$PtC_2B_8H_{10}$] species.[20] For this present work, initial nuclear magnetic shielding calculations were carried out for the conformations of $[(PMe_2Ph)_2PtC_2B_9H_{11}]$ implicit in Figure 4, using the GIAO technique and the 6-311+G(2d,p) basis sets for C, H, B and P, and the SDD basis set for Pt as found in Gaussian 03 package.[18] The calculated boron nuclear magnetic shieldings for $[(PMe_2Ph)_2PtC_2B_9H_{11}]$, expressed here in terms of ^{11}B NMR chemicals shifts $\delta(^{11}B)$/ppm, for the *trihapto*, *tetrahapto* and *pentahapto* conformations of $[(PMe_2Ph)_2PtC_2B_9H_{11}]$, together with the experimentally determined ^{11}B NMR chemical shift values $\delta(^{11}B)$ are given in Table 2, and are represented graphically in Figure 6 to aid visual comparison.

Table 2. Calculated boron nuclear magnetic shieldings, expressed as ^{11}B NMR chemical shifts $\delta(^{11}B)$/ppm, for the *trihapto*, *tetrahapto* and *pentahapto* conformations of $[(PMe_2Ph)_2PtC_2B_9H_{11}]$ and the experimentally determined ^{11}B NMR chemical shift values $\delta(^{11}B)$ for $[(PMe_2Ph)_2PtC_2B_9H_{11}]$ (data from reference 15).

assignment	*trihapto*	*tetrahapto*	*pentahapto*	mean of *trihapto* and *tetrahapto*	observed
B(4)		–15.9	–13.7		
B(4,7)	-22.6	–17.1	–12.6	–19.1	–20.8
B(7)		–18.4	–11.5		
B(5)		–28.7	–27.3		
B(5,11)	–8,5	–23.4	–27.7	–16.0	–14.5
B(11)		–18.1	–28.0		
B(6)	–27.6	–23.8	–23.8	–25.7	–20.8
B(8)	+14.3	–4.1	–13.0	+5.1	+5.7
B(9)		–0.7	–14.8		
B(9,12)	-9.9	–12.3	–12.5	–11.1	–9.9
B(12)		–23.9	–10.2		
B(10)	–9.8	–13.0	–10.5	–10.4	–9.2

It can be seen from the calculated values that there are substantial differences in the cluster shielding pattern among the three conformations (Figure 6, upper three diagrams). For the *tetrahapto* compared to the *trihapto* configurations the differences are principally for the B(8) position adjacent (α) to the metal atom and for the B(5,11) positions β to the metal atom, which both show shifts of some 20 ppm to higher shielding; concurrently there is a significant reduction in shielding at the B(4,7) positons α to the platinum centre, with the shieldings of other positions showing only minor changes. Differences on progression from the *tetrahapt*o to the *pentahapto* are not so marked, but there are again significant further increases in shieldings for the B(8) and B(5,11) positions; with the reduction in shielding at B(4,7) now more modest; again the other positons are little changed. These results may imply principal bonding changes involving molecular orbitals mainly involving the {Pt(3)B(4)B(7)B(8)B(5)B(11)} cluster domain as the rotation proceeds. None of these three individual shielding patterns maps well onto the experimentally determined ^{11}B chemical shift values for $[(PMe_2Ph)_2PtC_2B_9H_{11}]$ (Figure 6, bottom diagram), the principal differences being again at the α B(8), the α B(4,7) and the β B(5,11) sites just mentioned. Interestingly, however, a remarkably good match to the observed ^{11}B NMR spectrum is given by a mean of the calculated *trihapto* and *tetrahapto* values (penultimate diagram in Figure 6), which may imply that electronic and solution effects may make the *trihapto* and *tetrahapto* much closer in energy than the 8.8 kJ mol^{-1} calculated for the gas phase species, so that a time-average of the two is seen in solution, although this supposition has a number of the caveats.

[Figure 6 near here]

In accord with the supposition that changes in nuclear shieldings reflect changes in bonding, it was thence of further interest to examine at which stages along the rotational axis the significant changes in boron nuclear shielding and thence the significant changes in intracluster electronic bonding occur, and thence to see how this maps on to the changes in geometry through the *trihapto* and *tetrahapto* structures to the *pentahapto* transition state. The calculational time requirements were prohibitively large for the many incremental values required adequately to establish the nuclear magnetic shielding changes over the necessary quarter-rotation for 63-atom $[(PMe_2Ph)_2PtC_2B_9H_{11}]$, and so calculations were performed for the simpler model 31-atom species $[(PH_3)_2PtC_2B_9H_{11}]$ with 18 fewer non-hydrogen atoms. Confidence in that this would be representative of the triorganophosphine analogues derives from comparisons of the calculated shieldings within the *trihapto* 'parallel' mode for the PH_3, PMe_3 and PMe_2Ph species as illustrated in Figure 7. It can be seen that the general shielding behavioural pattern is very similar for all three compounds. Corresponding comparisons for each of the *tetrahapto* and *pentahapto* modes are correspondingly also very similar (Supplementary information).

[Figure 7 near here]

Figure 8 plots the variation with rotational angle of the calculated boron nuclear magnetic shieldings for the model compound $[(PH_3)_2PtC_2B_9H_{11}]$ for the first quarter-rotation. Figure S5 in the supplementary data shows the plot schematically extended for the full rotation by reflection and duplication. It can be seen from these two Figures that the nuclear magnetic shielding at the B(6) and B(10) positions β and γ to the metal centre show little significant change across the rotation. By contrast, the B(8) position adjacent (α) to the metal centre shows the biggest change, and the changes for the β-positioned B(5,11) and B(9,12) nuclei are also significant.

Interestingly, the B(4,7) positions α to the metal centre do not show such a large variation, but the changes are nevertheless noticeable. The two positions within each of the B(5,11) and B(9,12) pairs also show significant differential behaviour as the rotation moves towards asymmetric diagonal *tetrahapto* from the symmetrical parallel *trihapto* and perpendicular *pentahapto* conformations. There are two striking parallels with the structural variations seen in Figure 5 above, in that there are substantial areas of arc of about 40º or so around both the energy-minimum parallel and the energy-maximum perpendicular conformations, in each of which many of the shieldings are little changed, suggesting a constancy of electronic structure for much of the cluster over each of these quite extensive rotational arcs. There are then substantial changes over the 30 º or so of arc separating these two domains as the rotation passes through the diagonal conformation, implying concomitant rapid changes in cluster electronics in this region corresponding to the rapid structural changes represented in Figure 5. For this PH_3 model, there is no marked plateau of stability corresponding to the diagonal conformation, although there are deviations from monotonic behaviour around the relevant 40º/140º points, best seen in the partial plateau character of the B(9), B(10) and B(12) nuclear shieldings at these rotational angles; we would expect plateau behaviour to be manifested more strongly in the PMe_3 and PMe_2Ph compounds which exhibit structural energetic minima in that area. Within each of the parallel and the perpendicular conformational regions, comparison among Figures 2, 5 and 8 suggests that electronic aspects of bonding, as well as the geometrical aspects, do not change very much during energetic changes about 15 kJ mol^{-1} or so.

Conclusions

The above findings for the formally *closo* [3,3-$(PR_3)_2$-3,1,2-$PtC_2B_9H_{11}$] twelve-vertex systems confirm the previous supposition of a relatively unhindered contrarotation of the $\{Pt(PR_3)_2\}$ and *nido*-shaped carbons-together $\{C_2B_9H_{11}\}$ entities about an axis approximately defined by the Pt(3)–B(10) vector, with a transition from *trihapto* to *tetrahapto* to *pentahapto* metal-to-cluster interaction (schematics **XXX** → **XXXII** → **XXXII** respectively) as the rotation progresses from 0º to 90 º, and a reversal as it progresses in turn through to 180º, and thence through a similar cycle through to 360º for a complete rotation. The overall energy minimum is the *trihapto* mode **XXX**, but there is also an island of stability for the diagonal *tetrahapto* mode **XXXI** at slightly higher energy, corresponding to experimental observation of these two configurations. The highest-energy *pentahapto* mode **XXXII** constitutes a transition state, and its energy defines the activation energy for the complete contrarotation. The shallow minima and small energy differences suggest that ready cluster flexibility will be expected about the minima, induced by solvent effects in solution or packing effects in the solid state, again in accord with subtle rotamer angle differences seen when experimental results are compared. Nuclear magnetic shielding criteria suggest significant changes in intracluster bonding as the rotation progresses. The *trihapto* bonding geometry **XXX** and the corresponding electronic structure are favoured over quite a substantial arc (some 40º or so) of the rotation, before rapid changes ensue, and then, after progression through diagonal *tetrahapto* conformation **XXXI**, the electronics and, to some extent, the bonding geometry, then again remain similar within the *pentahapto* mode **XXXII** for a further 40º or so of the rotational arc about this rotational transition state.

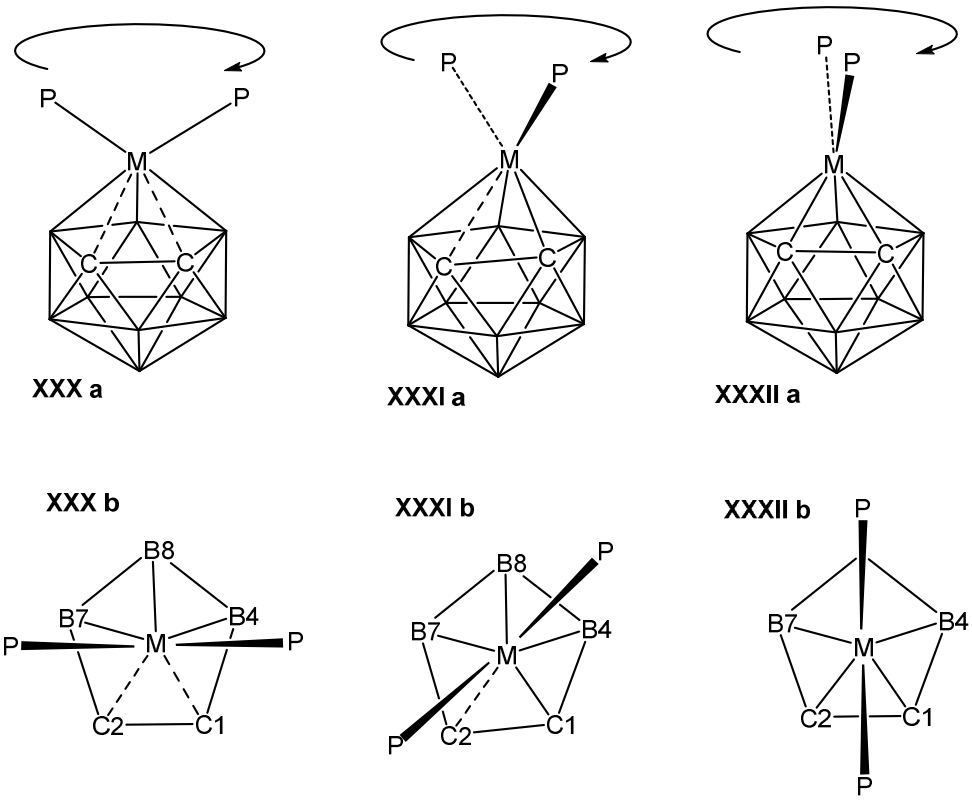

Experimental

All calculations were performed using the PBE hybrid functional (keyword PBE1PBE) method implemented in *Gaussian 03*, using the 6-31G(d) basis set for C, H, B and P, and the Stuttgart-Dresden ECP plus double zeta (SDD) basis set for Pt.[18] It has been reported that this functional provides accurate geometries for third-row transition metal elements.[21] Geometry optimizations were run without symmetry constraints, using regular convergence criteria. Vibrational frequencies were calculated to verify that the relevant stationary points were minima or transition states. The natures of the transition states were determined via the vibration analyses and concomitant visualization of the imaginary frequencies. Energies have zero-point energy corrections, with a scale factor of 0.9727.[22] Nuclear magnetic shielding calculations (GIAO method) were performed using the 6-311+G(2d,p) basis set for C, H, B and P, and the Stuttgart-Dresden ECP plus double zeta (SDD) basis set for Pt. The nuclear shieldings were initially presented as ^{11}B NMR chemical shifts relative to D_{2h} B_2H_6 (optimized at the PBE1PBE 6-31G(d) level, GIAO NMR calculations performed at the PBE1PBE 6-311+G(2d,p) level), which has a calculated shielding tensor of 86.5889 relative to the conventional ^{11}B NMR chemical shift standard taken as $[BF_3(OEt_2)]$ at a nominal +16.6 ppm.

Supplementary information

Comparative line-diagram plots of calculated boron nuclear shieldings of $[(PH_3)_2PtC_2B_9H_{11}]$, $[(PMe_3)_2PtC_2B_9H_{11}]$, and $[(PMe_2Ph)_2PtC_2B_9H_{11}]$; 360º compilation plots of variation of calculated interatomic distances and calculated nuclear magnetic shieldings with contrarotational angle for $[(PH_3)_2PtC_2B_9H_{11}]$; Tables of selected calculated and nuclear shieldings; Tables of selected calculated interatomic distances; Full citation for reference XX. (Gaussian)

Acknowledgements

Contribution no 129 from the Řež-Leeds Anglo-Czech Polyhedral Collaboration (ACPC). JDK thanks Professors S. Marsden, B. Štíbr and J. Bludská for their good offices.

References

1. M. F. Hawthorne, D. C. Young and P. A. Wegner, *J. Am. Chem. Soc.*, **1965**, *87*, 1818; M. F. Hawthorne and T. D. Andrews, *J. Am. Chem. Soc.*, **1965**, *87*, 2496; M. F. Hawthorne and R. L. Pilling, *J. Am. Chem. Soc.*, **1965**, *87*, 3987; M. F. Hawthorne and T. D. Andrews, *Chem. Commun*., **1965**, 443.
2. R. N. Grimes, *Carboranes, Second Edition*., 2011, Academic Press, London, New York, Amsterdam, and other cities.; ISBN 978-0-12-374170-7
3. R. M. Wing, *J. Amer. Chem. Soc*., 1967, **89**, 5599; and 1968, **90**, 4828; L. F. Warren and M. F. Hawthorne, *J. Amer. Chem. Soc*., 1968, **90**, 4823.
4. H. M. Colquhoun, T. J. Greenhough and M. G. H. Wallbridge, *J. Chem. Soc., Chem. Commun*., 1977, 737; *J. Chem. Soc., Dalton Trans*., 1979, 619.
5. A. J. Welch, *Chem. Commun*., 2013, 3615.
6. See, for example, J. Bould and R. Macías, *J. Organomet. Chem.,* 2014, **761**, 120.
7. J. D. Kennedy, *Disobedient Skeletons*, Chapter Three in *The Borane-Carborane-Carbocation Continuum*, Ed. J. Casanova, Wiley, New York, 1998, pp 85–116; ISBN: 0-471-18075-0
8. See, for example, L. S. Alekseev, F. M. Dolgushin and I. T. Chizhevsky, *J. Organomet. Chem*., 2008, **693,** 3331; L. S. Alekseev, A. V. Safronov, F. M. Dolgushin, A. A. Korlyukov, I. A. Godovikov and I. T. Chizhevsky, *J. Organomet. Chem*., 2009, **694** 1727.
9. J. Bould and J. D. Kennedy, *J. Organomet. Chem.,* 2014, **749**, 163.
10. See, for example, M. F. Hawthorne and K. P. Callahan, *Adv. Organomet. Chem*., 1976, **14**, 145.
11. P. A. Wegner, *Inorg. Chem*., 1975, **14,** 212; H. M. Colquhoun T. J. Greenhough and M. G. H. Wallbridge, *J. Chem. Soc., Chem. Commun*., 1976. 1019; W. E Carrol, M. Green, F. G. A. Stone and A. J. Welch, *J. Chem. Soc., Dalton Trans*., 1975, 2263; A. J. Welch, *J. Chem. Soc., Dalton Trans*., 1975, 1473; D. M. P. Mingos, *J. Chem. Soc., Dalton Trans*., 1977, 602.
12. D. M. P. Mingos, M. L. Forsyth and A. J. Welch, *J. Chem. Soc., Chem. Commun*., 1977, 605; *J. Chem. Soc., Dalton Trans*., 1978, 1363.
13. D. O'Connell, T. R. Spalding, G. Ferguson, J. F. Gallagher and J. D. Kennedy, *J. Organomet. Chem*., 1995, **503,** C12.
14. See, for example, G. Ferguson, J. F. Gallagher, J. D. Kennedy, D. O'Connell, J. C. Patterson and T. R. Spalding, *Acta Crystallogr., Sect. C*, 2005, **C61**, m393, and references therein.
15. G. Ferguson, J. F. Gallagher, Yi Wei, D. P. O'Connell, J. C. Patterson, T. R. Spalding, J. D. Kennedy, R. Macías and B. Štíbr, *J. Chem. Soc., Dalton Trans.*, 1996, 3323.
16. M. McGrath, T. R. Spalding, X. L. R. Fontaine, J. D. Kennedy and M. Thornton-Pett, *J. Chem. Soc., Dalton Trans.*, 1991, 3223.

17. M. Bühl, D. Hnyk and J. Macháček, *Chem. Eur. J.,* 2005, **11**, 4109; M. Bühl, J. Holub, D. Hnyk and J. Macháček, *Organometallics*, 2006**, 25***,* 2173

18. *Gaussian 03*, Revision B.04, Frisch, M. J; Pople, J. A; et al., Gaussian, Inc., Wallingford , CT, USA, 2004. For full citation, see supplementary supporting data.

19. H. M. Colquhoun, T. J. Greenhough and M. G. H. Wallbridge, *J. Chem. Soc., Dalton Trans*., 1985, 761.

20. J. D. Kennedy, B. Štíbr, M. Thornton-Pett, and T. Jelínek, *Inorg. Chem.*, 1991, **30**, 4481; J. D. Kennedy, B. Štíbr, T. Jelínek, X. L. R. Fontaine, and M. Thornton-Pett, *Collect. Czech. Chem. Commun*., 1993, **58***,* 2090; J. Bould, X. L. R. Fontaine, I. Cisařová and J. D. Kennedy, *Organometallics, F. G. A. Stone Memorial Edition*, 2012, **31**, 2691.

20. M. Bühl, C. Reimann, D. A. Pantazis, T. Bredow and F. Neese, *J. Chem. Theory Comput*. **2008**, *4*, 1449.

21. Y. Tantirungrotechai, K. Phanasant, S. Roddecha, P. Surawatanawong, V. Sutthikhum, J. Limtrakul, *J. Mol. Struct. Theochem*. **2006**, *760*, 189.

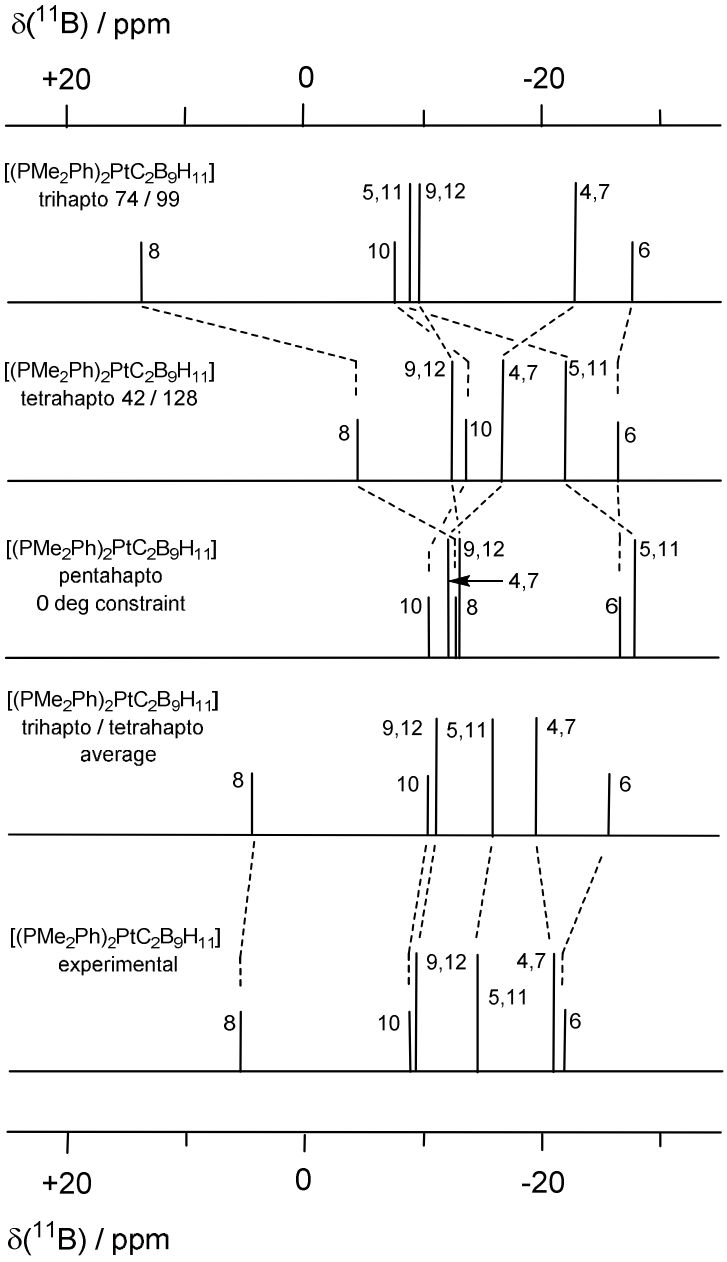

Figure 6. Representations of the boron nuclear magnetic shieldings, expressed as ^{11}B NMR chemical shifts $\delta(^{11}B)$, and relative intensities, as calculated for the *trihapto*, *tetrahapto* and *pentahapto* conformations of $[(PH_3)_2PtC_2B_9H_{11}]$ (upper three diagrams), the mean of the *trihapto* and *tetrahapto* values (fourth diagram), and the experimentally determined ^{11}B NMR chemical shift values $\delta(^{11}B)$ for $[(PMe_2Ph)_2PtC_2B_9H_{11}]$ (bottom diagram; data from reference 15). The calculated values are averaged across the idealised {Pt(3)B(8)B(6)B(10)} plane to reflect that the fluxionality gives time-averaged effective mirror plane symmetry on the NMR timescale.

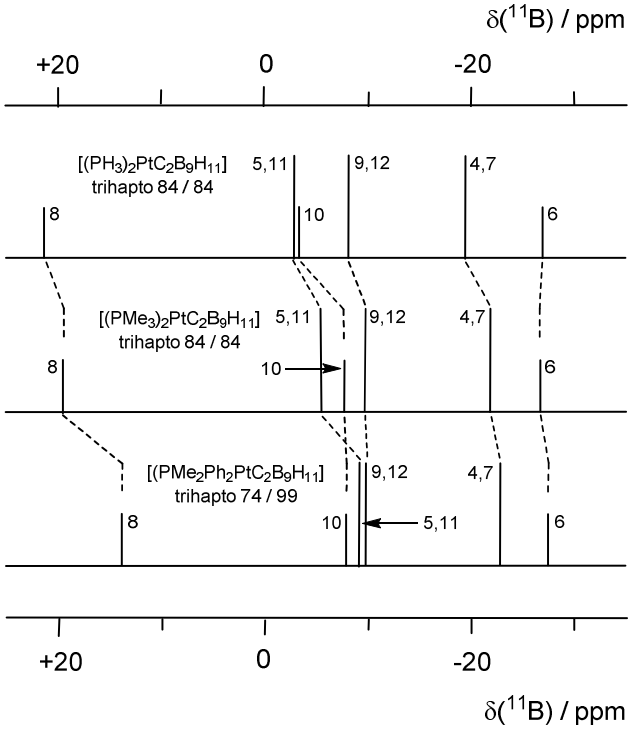

Figure 7. Representations of the boron nuclear magnetic shieldings, expressed as ^{11}B NMR chemical shifts δ(^{11}B), and relative intensities, as calculated for the *trihapto* 'parallel' conformations of $[(PH_3)_2PtC_2B_9H_{11}]$ (top diagram) $[(PMe_3)_2PtC_2B_9H_{11}]$ (middle diagram) and $[(PMe_2Ph)_2PtC_2B_9H_{11}]$ (lower diagram). Each of the (4,7), (5,11) and (9,12) pairs is averaged and combined to reflect that they would be exchanging positions by libration across the notional Pt(3)B(6)B(8)B(10) plane. See deposited supplementary data S2, S3 and S4 for the non-averaged plot, and for equivalent plots for the diagonal and perpendicular conformations.

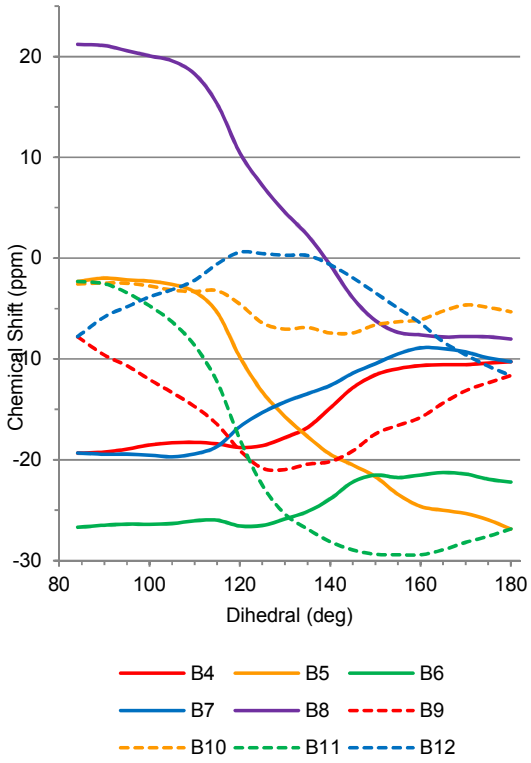

Figure 8 Variation with rotational angle of the calculated boron nuclear magnetic shieldings for the model compound $[(PH_3)_2PtC_2B_9H_{11}]$, expressed as boron NMR chemical shift values $\delta(^{11}B)$/ppm. For economy, calculations were performed only for the 84º effective quarter-rotation. The behaviour will combine with its mirror to give a half rotation, and the combination repeated to represent a complete 360º rotation (supplementary data, Figure S5).